Journal of the Optical Society of America A
OPTICS, IMAGE SCIENCE, AND VISION

Ultra-low-loss hollow-core anti-resonant fiber

Qiang Liu,[1] Peiqing Xing,[1] Yudan Sun,[2] Xiaotian Yao,[1] Guangrong Sun,[3] Tingting Lv,[1] Jingwei Lv,[1] Paul K. Chu,[4,5,6] and Chao Liu[1,*]

[1]School of Physics and Electronic Engineering, Northeast Petroleum University, Daqing 163318, China
[2]College of Mechanical and Electrical Engineering, Daqing Normal University, Daqing 163712, China
[3]College of Advanced Interdisciplinary Studies, National University of Defense Technology, Changsha 410073, China
[4]Department of Physics, City University of Hong Kong, Tat Chee Avenue, Kowloon, Hong Kong SAR, China
[5]Department of Materials Science and Engineering, City University of Hong Kong, Tat Chee Avenue, Kowloon, Hong Kong SAR, China
[6]Department of Biomedical Engineering, City University of Hong Kong, Tat Chee Avenue, Kowloon, Hong Kong SAR, China
*msm-liu@126.com

Received 2 September 2025; revised 20 October 2025; accepted 20 October 2025; posted 21 October 2025; published 13 November 2025

In this paper, an ultra-low-loss hollow-core anti-resonant fiber (HC-ARF) operating in the near-infrared band is proposed. The ARF is based on six nested circular tubes made of silica. Then a straight rod is added to the nested inner circular tube to reduce the transmission loss. The low-loss transmission performance of the HC-ARF is analyzed in detail using the finite element method, and the structural parameters are further optimized. The results show that the confinement loss is lower than 7.91×10^{-7} dB/m in the range of 1.54–1.78 μm. Especially the confinement loss is as low as 1.31×10^{-7} dB/m at 1.55 μm. In addition, the HC-ARF has good bending resistance. The bending loss can be kept below 8.02×10^{-5} dB/m as the bending radius is larger than 5 cm. The performance of the designed ARF is significantly better than previously reported results, and the cladding structure of the ARF is simple and easy to process. It has great potential for commercial applications.

https://doi.org/10.1364/JOSAA.576439

1. INTRODUCTION

With the rapid development of information technology, the higher transmission capacity of fiber-optic communication systems is required [1]. However, the traditional solid-core optical fiber restricts the expansion of communication capacity due to the nonlinear Shannon limit [2]. In order to overcome the material defects of solid optical fibers, hollow-core optical fibers as the light-conducting medium have been proposed and widely studied. The hollow-core optical fiber has the advantages of low delay, low dispersion, low nonlinearity, and high power damage threshold. It is a potential ideal transmission optical fiber, which can replace the traditional solid optical fiber and break through the capacity limit. Moreover, the hollow-core optical fibers also have a broad application prospect in other fields, such as gas sensing [3], mid-infrared transmission [4], precision machining [5], nonlinear optics [6], high harmonic generation [7], and refractive index sensor [8–10].

Hollow-core optical fibers mainly include photonic bandgap fibers [11–14] and anti-resonant fibers [15]. The hollow-core photonic bandgap fibers (HC-PBGFs) make use of the periodically arranged air holes in the cladding to confine the light in the core, and the propagation loss can be reduced by optimizing the structure of the cladding air holes. But the propagation bandwidth of HC-PBGFs is usually limited, whereas HC-ARFs use the anti-resonance effect and mode coupling suppression principle to confine the light in the fiber core, and can achieve low-loss transmission over a wide transmission bandwidth, thus effectively improve the information transmission capacity. In recent years, some HC-ARFs operating in the near-infrared band have been manufactured and tested in the experiment, such as Belardi and Knight achieved a multi-tube single-layer HC-ARF with a core diameter of 109 μm. The transmission loss at 3.1 μm is 0.1 dB/m [16]. In order to improve the transmission performance of the HC-ARFs, researchers have conducted extensive researches in the near-infrared band. Kolyadin *et al*. proposed an eight-tube node-free single-layer HC-ARF, the simple cladding structure exhibits lower transmission loss of 5×10^{-2} dB/m at 3.39 μm [17]. Subsequently, the nested HC-ARFs were proposed successively. Poletti analyzed the effect of the nested HC-ARF on the transmission performance and confirmed that the added nested tubes can effectively suppress the coupling between core and cladding modes and enhance the bending stability of HC-ARF. The minimum loss of the designed six-tube ARF is only 2×10^{-4} dB/m at 1.2 μm [18]. In addition, Zhang *et al*. fabricated a five-tube nested HC-ARF with the loss of 8.5×10^{-4} dB/m [19]. Recently, the double-nested structures are widely studied to further decrease the confinement loss. Gao *et al*. proposed double-circular-nested HC-ARF whose confinement loss is 1.3×10^{-4} dB/m [20]. In addition to the aforementioned single-layer and nested

structures based on circular tubes, researchers have also carried out extensive explorations of HC-ARFs with different geometries. Zhu *et al.* designed a novel HC-ARF: its cladding tubes consist of curves, and the minimum confinement loss is 6.58×10^{-5} dB/m at 1.06 μm [21]. Chen *et al*. proposed an elliptical nested HC-ARF with the confinement loss of 1.22×10^{-5} dB/m at 1.948 μm. The bending loss is less than 5.0×10^{-5} dB/m when the bending radius is greater than 15 cm [22]. Zhao *et al*. proposed a novel quad-tube HC-ARF, its cladding tube contains four nested inner tubes, and the confinement loss is 9.0×10^{-6} dB/m at 1.55 μm [23]. Gong and Meng designed a novel five-tube double-nested C-type HC-ARF with the confinement loss of 1.4×10^{-6} dB/m at 1.55 μm [24].

Comparing the above studies, it is found that the complex multi-layer nested structure can effectively decrease the confinement loss, but increase the difficulty of drawing ARF. In this paper, a novel ultra-low-loss HC-ARF is proposed by nesting a straight rod inside the inner circular cladding tubes. The simple cladding structure effectively decrease the confinement loss to 7.91×10^{-7} dB/m in the range of 1.54–1.78 μm. Meanwhile, the ARF exhibits good bending resistance and has broad application potential.

2. FIBER STRUCTURE

The cross section of the proposed HC-ARF is shown in Fig. 1. The cladding consists of six pairs of nested circular tubes with straight rods in the inner circular tubes. The white region is air with a refractive index of 1. The diameter of the fiber core is $D = 55$ μm. The wall thickness of the nested circular tubes is $t = 0.34$ μm. The diameters of the nested outer and inner circular tubes are d_1 and d_2, respectively. The values are changed with D; the relations are $d_1/D = 0.8$ and $d_2/d_1 = 0.7$. The thicknesses of the outer cladding and perfectly matched layer are $JT = 4$ μm and $T = 6$ μm, respectively. The material of the anti-resonator tube and the outer cladding part (blue area) is silica glass, the refractive index can be calculated by the Sellmeier [25] equation. The parameters are shown in Table 1.

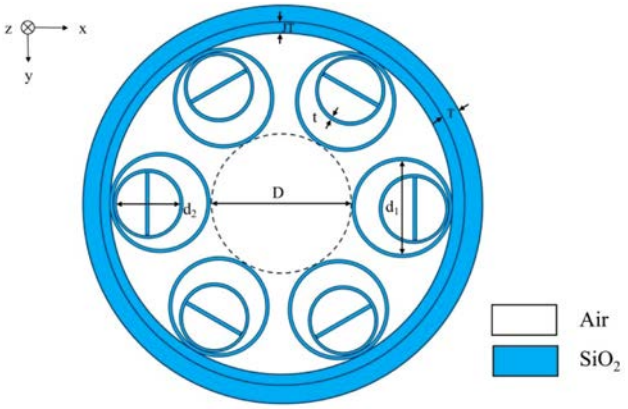

Fig. 1. Cross section of the ARF.

Table 1. Parameters of Fiber Structure

D	t	d_1/D	d_2/D	JT	T
55 μm	0.34 μm	0.8	0.7	4 μm	6 μm

The possible manufacturing methods of anti-resonant fiber include stacking [26], extrusion [27], and 3D printing [28]. The extrusion method is easily to deform the cladding tubes. The stacking method and 3D printing method can be used to fabricate the proposed anti-resonant fiber in the future. Then the finite element software COMSOL is used to analyze the performance of the HC-ARF. To ensure accurate numerical calculation using the finite element method, very fine grid sizes of $\lambda/6$ and $\lambda/4$ are used for the silica glass and air, respectively. The perfectly matched layer (PML) [29] is added outside the ARF as absorbing boundary condition.

3. RESULTS AND DISCUSSION

The effective refractive index n_1 of the silica glass can be solved by Sellmeier's [25] formula:

$$n_1^2(\lambda) = 1 + \sum_{j=1}^{m} \frac{B_j \lambda^2}{\lambda^2 - \lambda_j^2}, \tag{1}$$

where λ_j is the jth resonant wavelength, and B_j is the intensity of the jth resonant wavelength. The first three terms are usually used, and the parameters are shown in Table 2.

The anti-resonant condition can be obtained using the principle of light $\Delta\Phi = \Phi_1 - \Phi_0 = (2m-1)\pi$. As shown in Fig. 2, as the wavelength λ is much smaller than the fiber core diameter D, the longitudinal wave vector k_L can be approximated by $n_0 k_0$, and the transverse wave vector k_T in the glass region can be approximated by $kT = k_0(n_1^2 - n_0^2)^{1/2}$. Here, n_1 and n_0 are the refractive indices of glass and air, respectively. The parameter $k_0 = 2\pi/\lambda$ denotes the wave vector in the air. The phase difference between the waves passing through the glass slab with and without additional reflections is $2tk_0(n_1^2 - n_0^2)^{1/2}$. The anti-resonance condition that the phase difference is a multiple of $(2m-1)\pi$ is [30–33]

$$t = \frac{(m-0.5)\lambda}{2\sqrt{n_1^2 - n_0^2}}. \tag{2}$$

We mainly consider confinement loss (CL) and absorption loss of material. For HC-ARF, the light energy is concentrated in the hollow-core region, and the absorption loss of the material is negligible [34]. The confinement loss refers to the power

Table 2. Parameters of Sellmeier

$B_1 = 0.6961663$	$B_2 = 0.4079426$	$B_3 = 0.8974794$
$\lambda_1 = 0.0684043$	$\lambda_2 = 0.1162416$	$\lambda_3 = 9.896161$

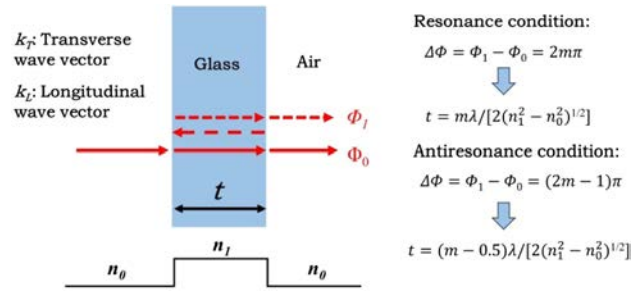

Fig. 2. Schematic illustration of the resonance and anti-resonance conditions.

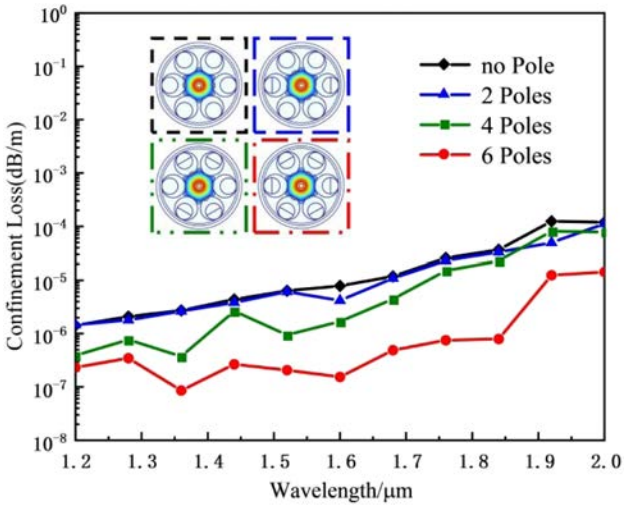

Fig. 3. Loss spectra for different straight rods.

loss caused by optical field leakage and is intrinsic to the ARF. Therefore, the confinement loss plays the main factor for transmission loss; the formula of calculating CL can be expressed as [33,35–37]

$$\mathrm{CL\ (dB/m)} = -\frac{20}{\ln 10}\frac{2\pi}{\lambda}\mathrm{Im}(n_{\mathrm{eff}}), \tag{3}$$

where $\mathrm{Im}(n_{\mathrm{eff}})$ represents the imaginary part of the effective refractive index, and λ is the wavelength of the incident light.

In order to study the effect of the straight rods on the confinement loss of the ARF, we first compare the CLs for different number of the rod as the initial parameters of the structure are $D = 55$ μm, $t = 0.34$ μm, $d_1/D = 0.8$, and $d_2/d_1 = 0.7$. The simulation result is shown in Fig. 3. It can be seen that the light field is well confined in the fiber core, and the structure based on nested circular cladding tubes exhibits lower CL of 10^{-5} dB/m, and the CL increases to 10^{-4} dB/m with increasing the wavelength. As the number of straight rods inserted to the inner circular cladding tubes is changed from 2 to 6, the CLs decrease gradually. The lowest CL reaches the level of 10^{-7} dB/m in the range of 1.2–2.0 μm. It means that three anti-resonance layers can better suppress light leakage and decrease the CL. Meanwhile, the simple structure is easily manufactured and achieved in the experiment.

Second, the effect of the wall thickness t of the cladding tubes on the CL is investigated. The thickness t determines anti-resonant wavelength. When $D = 55$ μm, $d_1/D = 0.8$, and $d_2/d_1 = 0.7$, the CLs for different wall thicknesses are shown in Fig. 4(a). It can be seen that the CLs are the highest as $t = 0.19$ μm. The CLs gradually decrease when the wall thickness t of the cladding tubes gradually increases from 0.19 to 0.29 μm. As t is 0.29 and 0.34 μm, the difference of the two loss spectra is smaller near 1.55 μm. To further get the optimal t, Fig. 4(b) shows the CLs at 1.55 μm for different wall thicknesses t and the corresponding mode field. The CLs exhibit fluctuant decrease and then relatively flat trend with the increase of the wall thickness t. Due to the lower CLs, the mode field schematic cannot distinguish the difference of the core mode energy leakage for different t. In order to achieve wider low-loss transmission bandwidth near 1.55 μm, $t = 0.34$ μm is chosen as the optimal value.

The influence of the diameter d_1 of the cladding circular tubes on the CLs is discussed. The decrease of d_1 results in the increase of D; therefore, d_1/D is adopted to analyze the performance of the ARF. Meanwhile, the diameter d_2 of the nested inner tubes decreases proportionally with d_1. The initial parameters are $D = 55$ μm, $t = 0.34$ μm, and $d_2/d_1 = 0.7$. Then the CLs for different d_1/D are calculated as shown in Fig. 5(a). It can be seen that the CLs are relative higher as d_1/D is 0.65 and decreases gradually with increasing d_1/D from 0.65 to 0.75. It indicates that the narrower spacing of the adjacent cladding tubers can better confine the core mode and decrease the CLs. As d_1/D is further increased, this effect is no longer significant. In order to get the optimal d_1/D, the CLs for different d_1/D at 1.550 μm are calculated as shown in Fig. 5(b), and the CLs decrease gradually with the increase of d_1/D. The equivalent line diagrams of core mode fields reflect the minor changes of the CLs. The smaller spacing can avoid energy leakage of the core mode; the ARF gets the minimum CL at $d_1/D = 0.8$.

The effect of the diameter d_2 of the nested inner layer circular tube on the CLs is investigated. As $D = 55$ μm, $t = 0.34$ μm,

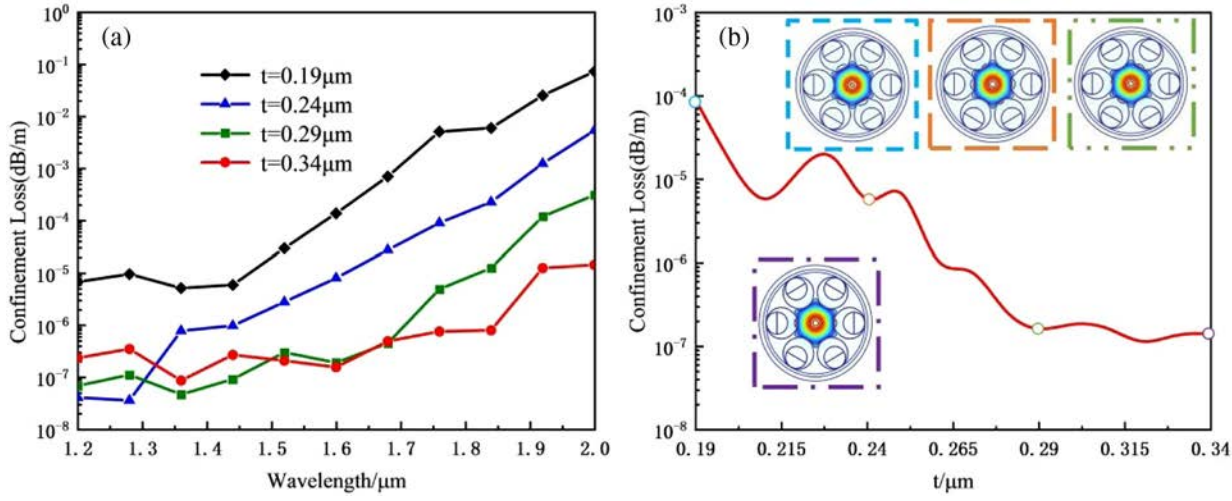

Fig. 4. (a) Wall thickness t of the cladding tubes versus wavelength; (b) CLs for different t at 1.55 μm.

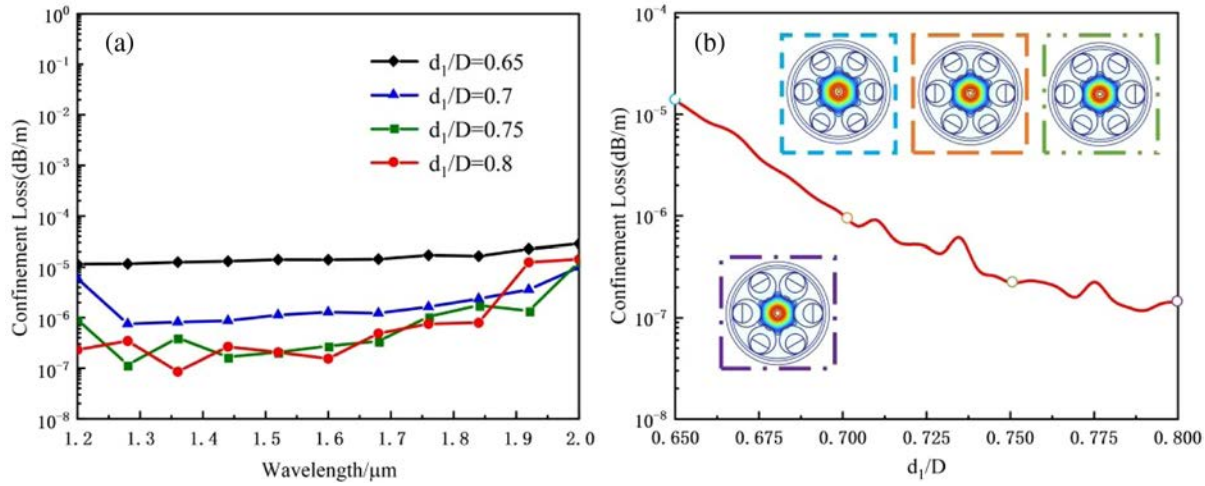

Fig. 5. (a) CLs versus wavelength for different d_1/D; (b) CLs for different d_1/D at 1.55 μm.

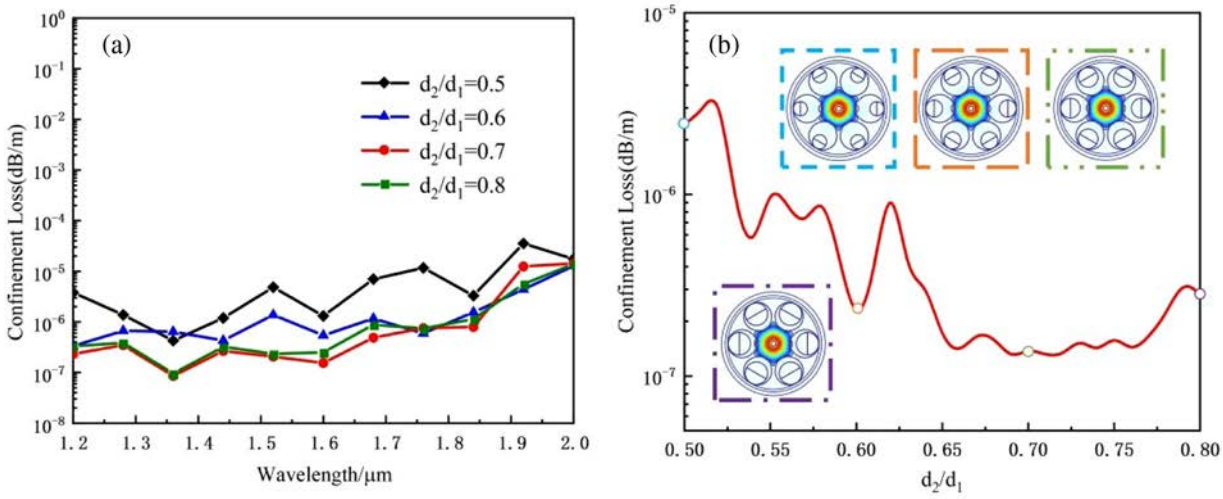

Fig. 6. (a) CLs versus wavelength for different d_2/d_1; (b) CLs for different d_2/d_1 at 1.55 μm.

and $d_1/D = 0.8$, Fig. 6(a) shows CLs for different d_2/d_1. It can be seen that the CLs of the ARF are reduced by an order of magnitude as d_2/d_1 gradually increases from 0.5 to 0.8. It indicates that the inner circular tube can form the second anti-resonance layer and suppress the core mode field, but the confinement ability is weaker as d_2 is smaller [38]. As d_2/d_1 are 0.7 and 0.8, the difference of the confinement loss spectra is smaller. Figure 6(b) shows the CLs for different d_2/d_1 at 1.55 μm. It can be seen that when d_2/d_1 is near 0.7, the electric field is better confined in the core region, and the CLs are lower. Therefore, $d_2/d_1 = 0.7$ is chosen as the optimal value.

When $D = 55$ μm, $t = 0.34$ μm, $d_1/D = 0.8$, and $d_2/d_1 = 0.7$, the effect of the number of nested circular tubes on the CLs is shown in Fig. 7. The ARF with four cladding tubes exhibits the largest losses, as shown by the black curve. The mode field diagram at 1.55 μm with black frame shows that the energy of the core mode leakage to the cladding. When the number of nested circular tubes is increased to five, the light field is well confined in the core region, whereas the ARF with six nested circular tubes further enhances the anti-resonance effect and reduces the CLs. As a result, the six nested circular tubes' structure is designed to construct the ARF with low-loss transmission characteristic.

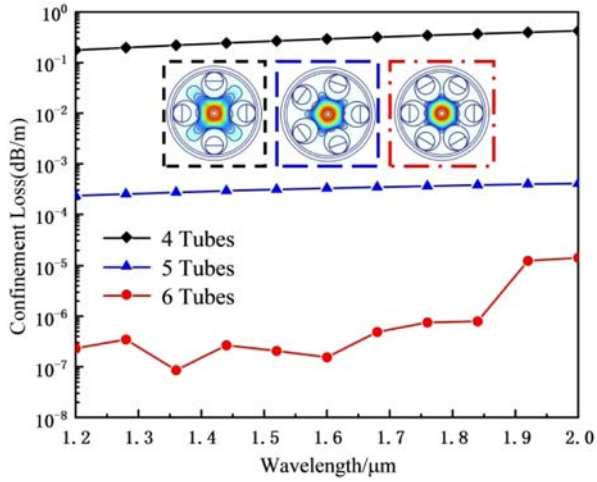

Fig. 7. Confinement loss spectra of different tube numbers.

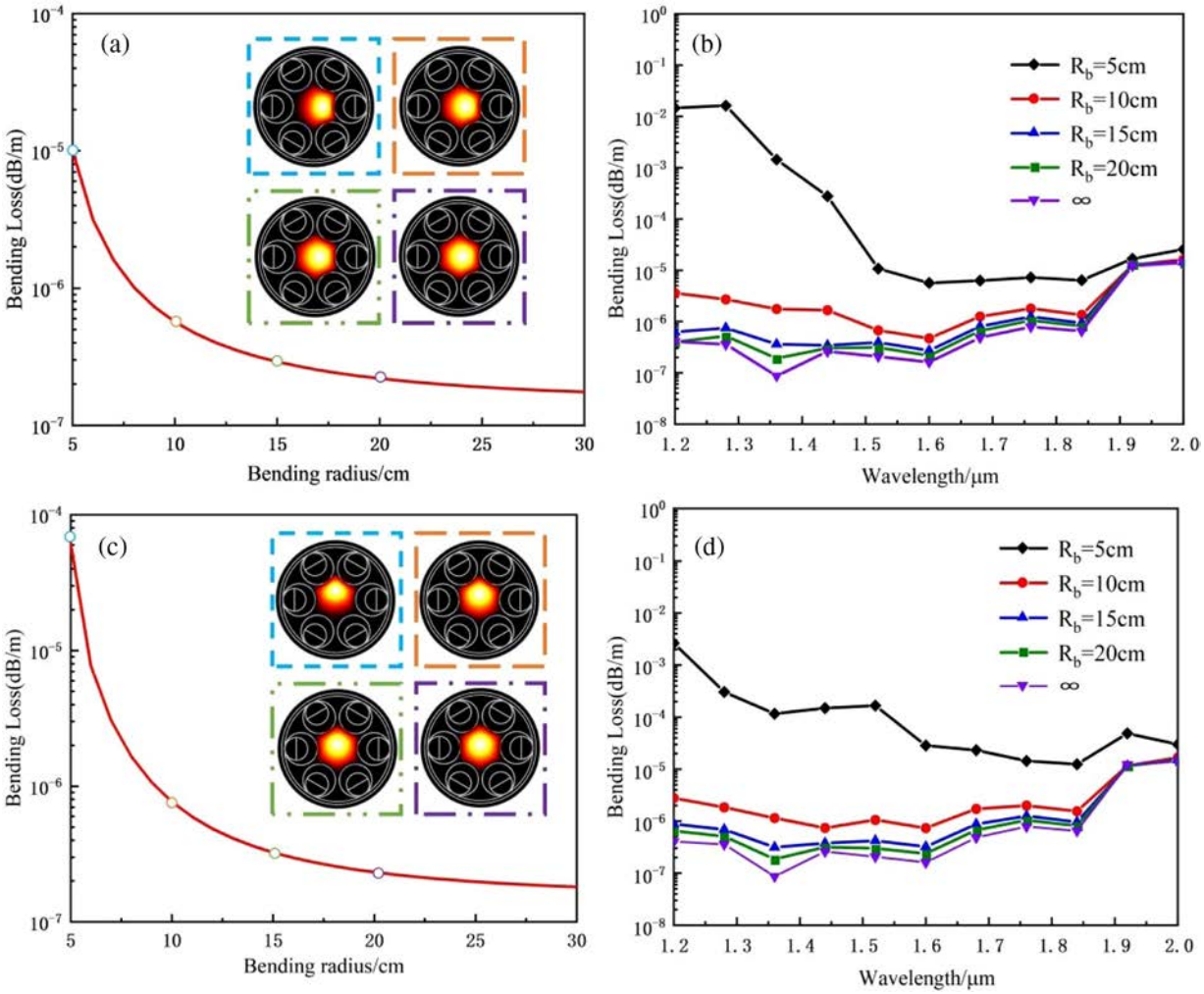

Fig. 8. (a) BL along the x axis at 1.55 μm, (b) BL spectra along the x axis for different bending radius, (c) BL along the y axis at 1.55 μm, and (d) BL spectra along the y axis for different bending radius.

Bending of optical fiber is unavoidable in practical application; it affects the communication quality directly. Since the structure of the designed HC-ARF is symmetric along the x axis and y axis, the bending loss (BL) can be calculated using the refractive index bending model [39]. The model can be simplified to the following equation [40,41]:

$$n_g = n(x, y)\left(1 + \frac{r}{R_b}\right), \tag{4}$$

where $n(x, y)$ is the refractive index of the straight fiber, r is the bending direction of the fiber (x or y), R_b is the bending radius, and n_g is the equivalent refractive index of the fiber after bending. Then the BL can be calculated by taking the n_g into Eq. (3).

The BLs of the proposed anti-resonant fiber are shown in Fig. 8. Figure 8(a) exhibits the BL along the x axis at 1.55 μm for different bending radius. As the bending radius R_b increases, the BL gradually decreases. It is because the bending destroys the symmetrical structure of the ARF and distorts the refractive index distribution, then the mode field gradually deviates from the center of the fiber core and leaks into the cladding as show in the inset. As the bending radius is 5 cm, the BL is only 5×10^{-5} dB/m. Figure 8(b) shows the corresponding BL spectra in the range of 1.2–2.0 μm. As the bending radius is smaller, the BL decreases first and then remains almost unchanged with increasing the wavelength. For larger bending radius, the influence of wavelength on bending loss is almost negligible. The proposed ARF exhibits excellent characteristic of bending resistance. Similarly, the bending characteristic along the y axis is shown in Figs. 8(c) and 8(d). Compared with the bending loss of the x axis, the low-loss bandwidth and the minimum loss show the same trend. At 1.55 μm, the BL along y axis is slightly smaller than that along x axis. The BL can be kept below 8.02×10^{-5} dB/m in the range 1.54–1.78 μm as the bending radius is greater than 5 cm. It can be seen that the bending loss can be maintained below 8.02×10^{-5} dB/m when the bending radius exceeds 5 cm. This demonstrates that the structure possesses excellent bending resistance characteristics.

4. CONCLUSION

In this paper, a novel HC-ARF with ultra-low confinement loss and bending loss operating in the near-infrared band is proposed. See Table 3. The simple cladding structure, which

Table 3. Comparison Between Our ARF and Previously Reported ARFs

Reference	Material Type	Confinement Loss (dB/m)	Operating Wavelength (μm)	Bending Loss (dB/m)
Ref. [16]	Silica	5.0×10^{-2}	3.39 μm	/
Ref. [18]	Silica	8.5×10^{-4}	2 μm	/
Ref. [19]	Silica	1.3×10^{-4}	1.55 μm	/
Ref. [21]	Silica	1.22×10^{-5}	1.948 μm	5.0×10^{-5} (>15 cm)
Ref. [23]	Silica	1.4×10^{-6}	1.55 μm	/
This work	Silica	1.31×10^{-7}	1.55 μm	8.02×10^{-5} (>5 cm)

consists of nested circular tubes and a straight rod, achieves ultra-low CL. The performance is optimized in detail using the FEM method. The results show that the CL is lower than 7.91×10^{-7} dB/m in the range of 1.54–1.78 μm and reaches 1.31×10^{-7} dB/m at 1.55 μm. In addition, the ARF shows an excellent bending resistance characteristic; the bending loss can keep below 8.02×10^{-5} dB/m as the bending radius is greater than 5 cm. The proposed structure provides a new method for the design of hollow-core optical fibers.

Funding. Excellent Youth Scholars of Heilongjiang Province (YQJH2023077); National Natural Science Foundation of China (12304480); Natural Science Foundation of Heilongjiang Province (JQ2023F001); Local Universities Reformation and Development Personnel Training Supporting Project from Central Authorities, Natural Science Foundation of Heilongjiang Province (LH2021F007); China Postdoctoral Science Foundation (2020M670881); City University of Hong Kong Strategic Research Grant (SRG) (7005505); City University of Hong Kong Donation Research Grant (DON-RMG 9229021).

Disclosures. The authors declare no conflicts of interest.

Data availability. Data underlying the results presented in this paper are not publicly available at this time but may be obtained from the authors upon reasonable request.

REFERENCES

1. W. Shi, Y. Tian, and A. Gervais, "Scaling capacity of fiber-optic transmission systems via silicon photonics," Nanophotonics **9**, 4629–4663 (2020).
2. W. Q. Zhang, T. H. Chan, and V. S. Afshar, "A correlation propagation model for nonlinear Fourier transform of second order solitons," Sci. Rep. **11**, 2434 (2021).
3. Y. Li, H. Chen, and Q. Chen, "Surface plasmon resonance induced methane gas sensor in hollow core anti-resonant fiber," Opt. Fiber Technol. **78**, 103293 (2023).
4. W. Chen, S. Qiao, and Y. He, "Mid-infrared all-fiber light-induced thermoelastic spectroscopy sensor based on hollow-core anti-resonant fiber," J. Photoacoust. **36**, 100594 (2024).
5. A. I. Adamu, Y. Wang, and R. A. Correa, "Low-loss micro-machining of anti-resonant hollow-core fiber with focused ion beam for optofluidic application," Opt. Mater. Express **11**, 338–344 (2021).
6. A. Trenti, C. Luchian, and F. Poletti, "High fidelity distribution of telecom polarization entangled photons through a 7.7 km antiresonant hollow-core fiber," IEEE J. Sel. Top. Quantum Electron. **30**, 6400308 (2024).
7. S. M. Njoroge and D. M. Kinyua, "High-order harmonic generation in a doped semiconductor by inhomogeneous laser field," Appl. Phys. B. **130**, 110 (2024).
8. T. Chen, J. Gao, and X. Wang, "High FOM Fano resonance refractive-index sensor based on a baffled MIM waveguide coupled with an inverted L-Shaped resonator," Physica Scripta **100**, 015533 (2024).
9. H. Zhu, X. Wang, and Y. Chen, "Plasmonic refractive index sensor of a hexagonal close-packed gold nanodisk array coupled with a gold thin film," J. Opt. Soc. Am. B **42**, 1251–1257 (2025).
10. H. P. Pasanen, R. Khan, and J. A. Odutola, "Transient absorption spectroscopy of films: impact of refractive index," J. Phys. Chem. C **128**, 6167–6179 (2024).
11. K. Murakami, S. Sugiura, and H. Yamaji, "High-power analog radio-over-fiber transmission using a hollow-core photonic bandgap fiber," IEEE Photonics Technol. Lett. **36**, 709–712 (2024).
12. X. Yang, Q. Song, and C. Ma, "A methane concentration sensor with heightened sensitivity and D-shaped cross-section U-shaped channel utilizing the principles of surface plasmon resonance," Phys. E **161**, 115954 (2024).
13. T. Dai, Y. Yi, and Z. Yi, "Photonic crystal fiber based on surface plasmon resonance used for two parameter sensing for magnetic field and temperature," Photonics **11**, 784 (2024).
14. S. Cheng, W. Li, and H. Zhang, "High sensitivity five band tunable metamaterial absorption device based on block like Dirac semimetals," Opt. Commun **569**, 130816 (2024).
15. S. Fu, H. Xu, and H. Tian, "Large-mode-area Nd-doped anti-resonant phosphate fiber for high-power single-mode 900 nm laser generation," Opt. Express. **32**, 36240–36250 (2024).
16. W. Belardi and J. C. Knight, "Hollow antiresonant fibers with low bending loss," Opt. Express **22**, 10091–10096 (2014).
17. A. N. Kolyadin, A. F. Kosolapov, and A. D. Pryamikov, "Light transmission in negative curvature hollow core fiber in extremely high material loss region," Opt. Express **21**, 9514–9519 (2013).
18. F. Poletti, "Nested antiresonant nodeless hollow core fiber," Opt. Express **22**, 23807–23828 (2014).
19. X. Zhang, W. Song, and Z. Dong, "Low loss nested hollow-core anti-resonant fiber at 2 μm spectral range," Opt. Lett. **47**, 589–592 (2022).
20. S. Gao, H. Chen, and Y. Sun, "Fourfold truncated double-nested antiresonant hollow-core fiber with ultralow loss and ultrahigh mode purity," Optica **12**, 56–61 (2025).
21. Y. F. Zhu, X. Y. Zuo, and P. Yan, "Low-loss nodeless conjoined-tube anti-resonant hollow-core fiber," J. Lightwave Technol. **41**, 4831–4839 (2023).
22. J. Chen, L. Peng, and Y. Shi, "Nested hollow-core anti-resonant fiber with elliptical cladding for 2 μm laser transmission," Opt. Express **32**, 28148–28159 (2024).
23. X. Zhao, X. Wu, and X. Lan, "Adjacent nested 4-tube hollow-core anti-resonant fiber," Opt. Commun. **522**, 128631 (2022).
24. Y. Gong and Y. Meng, "Single-polarization single-mode broadband ultra-low loss hollow-core anti-resonant fiber with nested double C-type cladding tubes," Opt. Commun. **552**, 130062 (2024).
25. D. F. Santos, A. Guerreiro, and J. M. Baptista, "SPR microstructured D-type optical fiber sensor configuration for refractive index measurement," IEEE Sens. J. **15**, 5472–5477 (2015).
26. G. Zhenyu, N. Tigang, and P. Li, "Antiresonant fiber structures based on swarm intelligence design," Opt. Express **31**, 26777–26790 (2023).
27. W. Talataisong, J. Gorecki, and L. D. van Putten, "Hollow-core antiresonant terahertz fiber-based TOPAS extruded from a 3D printer using a metal 3D printed nozzle," Photonics Res. **9**, 1513–1521 (2021).
28. M. Rahman and M. Ordu, "Long-length 3D printed hollow-core polymer optical fiber for wideband light guidance," Opt. Fiber Technol. **81**, 103512 (2023).
29. D. Hou, X. Wang, and S. Lou, "Dual-hollow-core anti-resonant fiber with silicon layers and nested resonant tubes for constructing a single-polarization 3 dB coupler," Opt. Express **32**, 38780–38792 (2024).
30. C. Wei, R. J. Weiblen, and C. R. Menyuk, "Negative curvature fibers," Adv. Opt. Photonics **9**, 504–561 (2017).
31. S. Liu, L. Zhang, and M. Tian, "Epsilon negative-based, broadband single-polarization single-mode hollow core anti-resonant photonic crystal fiber," Opt. Express **29**, 15664–15677 (2021).

32. S. Jiang, P. Yang, and Z. Wang, "Dual-parameter sensor for temperature and strain measurement based on antiresonance effect and few-mode fiber," Photonics **10**, 642 (2023).
33. S. Liu, T. Yang, and L. Zhang, "An intensity demodulated refractive index sensor based on a hollow-core anti-resonant fiber," J. Phys. D **55**, 155107 (2022).
34. B. Gao, F. Tan, and D. Chen, "Design and study of low loss, high birefringence quasi-symmetric hollow-core anti-resonant fiber," Photonics **11**, 675 (2024).
35. W. Liu, Y. Shi, and Z. Yi, "Surface plasmon resonance chemical sensor composed of a microstructured optical fiber for the detection of an ultra-wide refractive index range and gas-liquid pollutants," Opt. Express **29**, 40734–40747 (2021).
36. Q. Liu, G. Sun, and Y. Sun, "Negative curvature fiber (NCF) polarization filter with large polarization loss ratio and ultralow loss in the terahertz range," Opt. Commun. **568**, 130736 (2024).
37. Q. Liu, G. Sun, and H. Mu, "Hybrid nested negative curvature fiber with ultra-low-loss in the terahertz band," Infrared Phys. Technol. **136**, 105003 (2024).
38. C. Wei, J. Hu, and C. R. Menyuk, "Comparison of loss in silica and chalcogenide negative curvature fibers as the wavelength varies," Front. Phys. **4**, 30 (2016).
39. J. Sultana, S. Islam, and C. M. B. Cordeiro, "Exploring low loss and single mode in antiresonant tube lattice terahertz fibers," IEEE Access **8**, 113309 (2020).
40. H. Liu, Y. Wang, and Y. Zhou, "Low bending loss few-mode hollow-core anti-resonant fiber with glass-sheet conjoined nested tubes," Opt. Express **30**, 21833–21842 (2022).
41. Q. Liu, G. Sun, and Y. Sun, "Anti-resonant fiber with high-resistivity silicon for THz wave transmission," J. Opt. Soc. Am. A **40**, 2128–2134 (2023).